Modeling of Residual Stresses in Core Shroud Structures

M. Mayfield, M. McNeil, US Nuclear Regulatory Commission
J. Zhang, P. Dong, F. W. Brust, Battelle Columbus Laboratories
W. J. Shack, Argonne National Laboratory

SMIRT 14, PCS 2, Lyon, August 25 and 26, 1997

This work was supported by the Office of Nuclear Regulatory Research, U.S. Nuclear Regulatory Commission, Job Code W-6610, Program Manager Michael McNeil.

DISCLAIMER

Modeling of Residual Stresses in Core Shroud Structures

J. Zhang, P. Dong, F. W. Brust, Battelle Columbus Laboratories
W. J. Shack, Argonne National Laboratory
M. Mayfield, M. McNeil, U.S. Nuclear Regulatory Commission

SMIRT 14, PCS 2, Lyon, August 25 and 26, 1997

Introduction

A BWR core shroud is a cylindrical shell that surrounds the reactor core. Feedwater for the reactor is introduced into the annulus between the reactor vessel wall and the shroud, as shown in Fig. 1. The shroud separates the feedwater from the cooling water flowing up through the reactor core. The shroud also supports the top guide which provides lateral support to the fuel assemblies and maintains core geometry during operational transients and postulated accidents to permit control rod insertion and provides the refloodable volume needed to ensure safe shutdown and cooling of the core during postulated accident conditions. Core shrouds were fabricated from welded Type 304 or 304L stainless steel plates and are supported at the top and bottom by forged ring support structures.

In 1990, cracking was reported in the core shroud of a non–U.S. BWR. The cracks were located in the heat–affected zone (HAZ) of a circumferential core shroud weld. Subsequent inspections in U.S. BWRs have revealed the presence of numerous flaw indications in some BWR core shrouds, primarily in weld HAZs. In several instances, this cracking was quite extensive, with the cracks extending 75% or more around the circumference of some welds. However, because the applied stresses on the shroud are low during operation and postulated accidents and because of the high fracture toughness of stainless steel, adequate structural margins can be preserved even in the presence of extensive cracking. Although assessments by the USNRC staff of the potential significance of this cracking have shown that core shroud cracking does not pose a high degree of risk in the short term, the staff concluded that the cracking was a safety concern for the long term because of the uncertainties associated with the behavior of core shrouds with complete 360° through–wall cracks under accident conditions and because it could eliminate a layer of defense–in–depth.

Core shrouds are subject to relatively low fluence, and most cases of core shroud cracking have been attributed to classical intergranular stress corrosion cracking (IGSCC) of thermally sensitized SS. Because the applied stresses on the shroud are very low, the nature of the cracking experienced by core shrouds is strongly influenced by residual stresses associated with the core shroud welds. As part of a USNRC research program on Environmentally Assisted Cracking of Light Water Reactor Materials at Argonne National Laboratory (ANL), Battelle Columbus Laboratories (BCL), under a subcontract from ANL, has calculated weld residual stresses and the associated stress intensity factors for BWR core shroud welds. The residual stresses were calculated with an axisymmetric finite–element model. A shell element analysis was also performed to quantify the effects of specimen removal on residual stress measurements. Based on the residual stress results obtained, stress intensity factors were calculated for complete circumferential cracks and for surface cracks with a finite aspect ratio. A detailed description of the weld residual stresses and associated stress intensity factors has been obtained for the H4 weld.

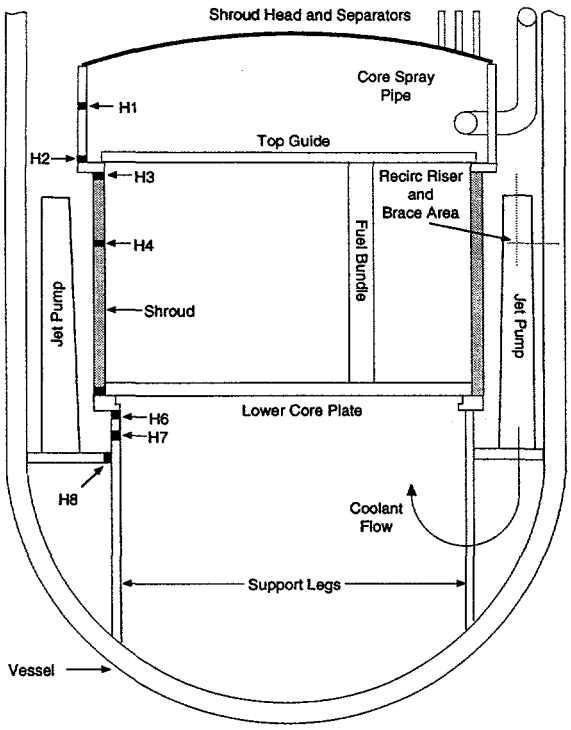

Figure 1
BWR reactor pressure vessel and internals

Core Shroud Weld Geometry and Calculation of Residual Stress Distributions

The H4 weld is a multipass submerged-arc weld that joins two Type 304 SS cylinders. The geometries of the cylinders and the H4 weld are shown in Fig. 2. The welding parameters are listed in Table 1, and an arc efficiency of 70% was assumed in calculating heat inputs. The root passes on the inner side of the cylinder were made first.

Based on the H4 weld geometry and pass sequence, an axisymmetric finite–element model was generated, as shown in Fig. 3. The finite–element model consists of 2952 elements and 3145 nodes. A refined mesh was used in and near the weld region. In the weld region, 18 lumped weld passes were assumed, as indicated in Fig. 3b where Passes 1 and 10 are the root passes on the inner and outer sides of the cylinder. A thermal analysis was performed using the TEMPER code developed at BCL, and the temperature solutions obtained from the thermal analysis were then used as input for the structural analysis, which was performed with the ABAQUS finite–element code. Currently, almost all general-purpose commercial finite–element codes, including ABAQUS, are incapable of directly modeling welding phenomenon such as material melting and metal deposition. A special user–material subroutine was developed at BCL to model material behavior during welding.

The H4 weld temperature history generated by TEMPER was read into the special user subroutine to calculate the driving force for the mechanical analysis. The sequential metal deposition effects associated with multiple passes are simulated by assigning to those filler elements that are not yet deposited a negligible material stiffness (comparable to the stiffness at melting temperature). Once a filler element is deposited, its stiffness is restored. The material properties are assumed to be temperature-dependent with nonlinear hardening behavior.

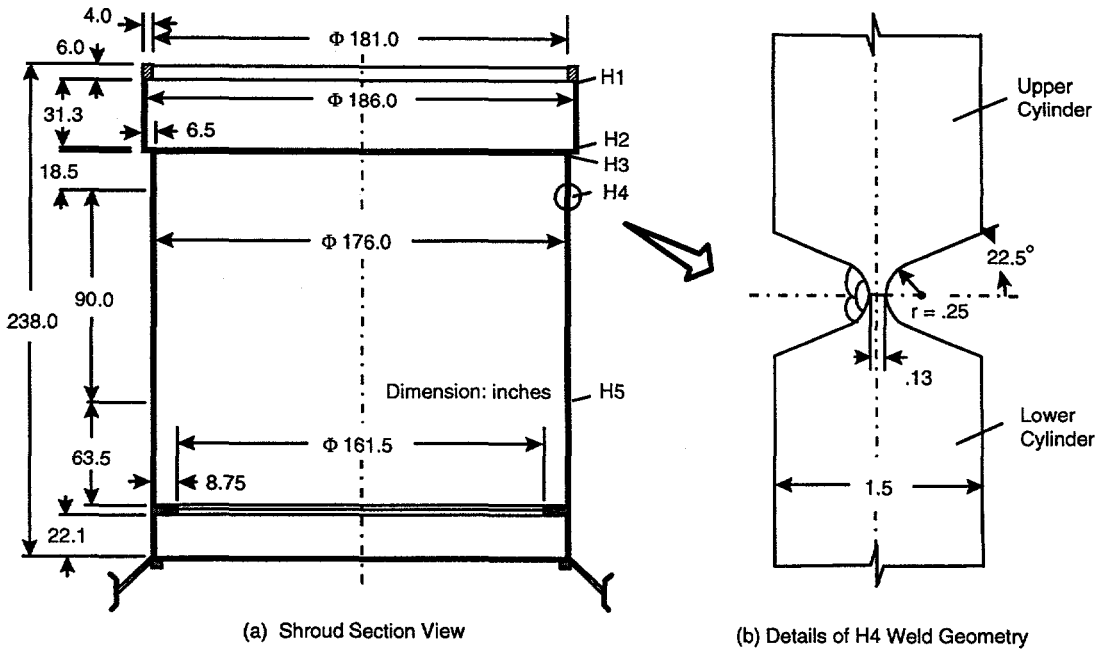

Figure 2. Core shroud structure and H4 weld geometry

Table 1. Welding parameters for H4 weld

Passes	Current (A)	Voltage (V)	Travel Speed (mm/s)
Root	285	28	6.3
Balance	510	30	7.6

Figure 4a shows the resulting axial residual stress distributions through the thickness of shroud wall at the weld centerline (Y = 0) and heat-affected zones (HAZs) (Y = –19–mm [-0.75–in.], 19–mm [0.75–in.]). The axial residual stresses show a "thick-shell" type of distribution. At both inner and outer surfaces of the pipe, tensile stresses are present, except at the weld centerline where a small-amplitude compressive stress is present on the outer surface. In the middle of the wall, the axial residual stresses are compressive. This compressive axial stress was primarily due to axial bending of the wall caused by radial shrinkage of the weld and the presence of weld cap. At the HAZs (19–mm [0.75–in.] away from the weld centerline), tensile stresses occur at both the inner and outer surfaces. The stress distributions at the two HAZ locations are very similar except near the outer surface. The difference near the outer surface is primarily due to the effects of the weld pass sequence in the last weld layer (Passes 16, 17 and 18). At the HAZ cross sections, the maximum tensile axial stresses are at the inner surface of the shroud wall.

Figure 4b shows the corresponding throughwall hoop residual stress distributions. As expected, the hoop stresses are tensile almost everywhere at these cross sections. The maximum tensile hoop stress occurs at the weld centerline between the midthickness and outer surfaces. At the HAZs, the tensile stresses peak at the inner and outer surfaces; however, their magnitudes are much smaller than the peak value at the weld centerline.

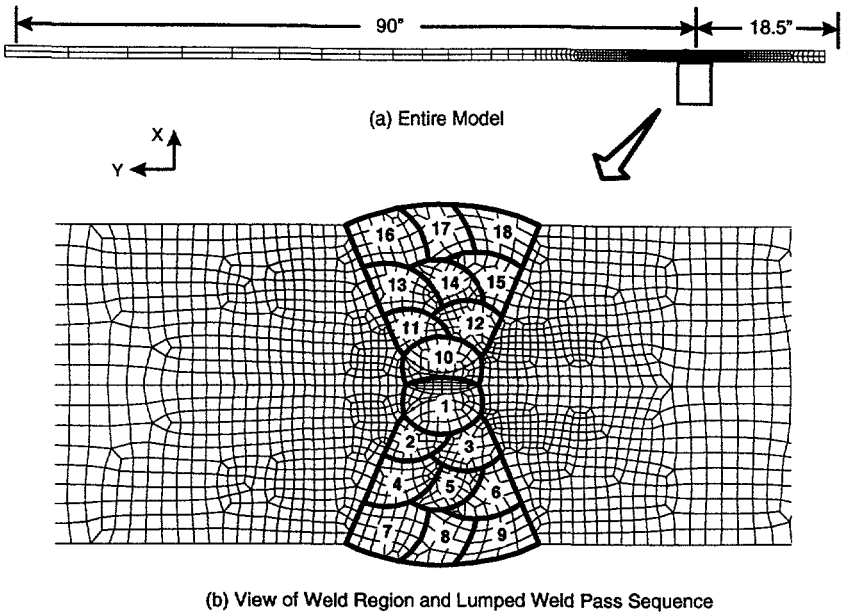

Figure 3. Axisymmetric finite-element model for H4 weld analysis

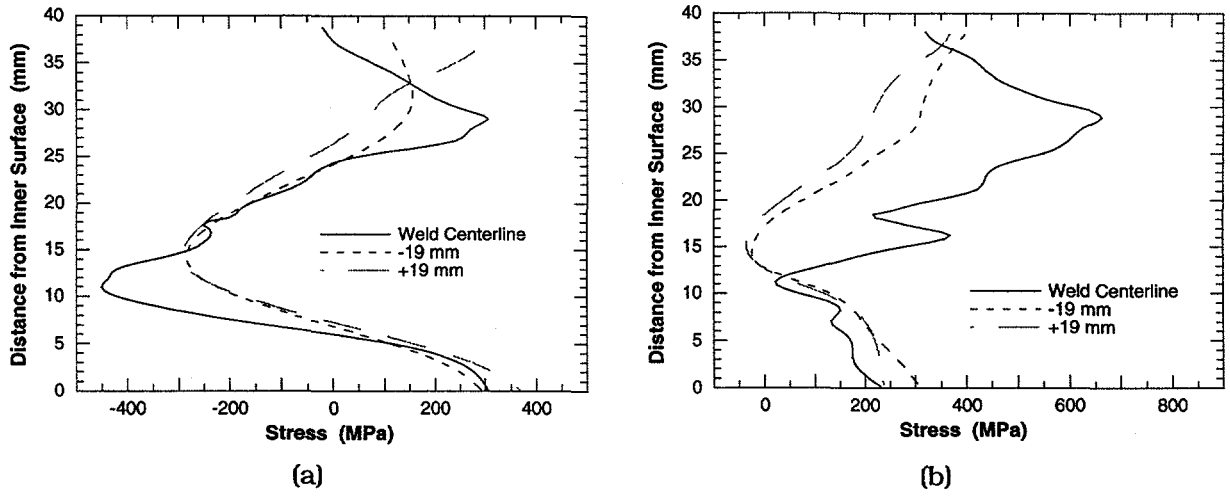

Figure 4. Throughwall residual stress distribution in H4 Weld (a) axial stress, (b) hoop stress

Figures 5a and 5b shows contour plots of the axial and hoop residual stresses for an axial cross-section through the weld. Fig. 6a shows the axial residual stress distributions along the outer and inner surfaces of the shroud. The hoop residual stress distributions at the inner and outer surfaces are shown in Fig. 6b. The hoop stresses are tensile within the weld area and decrease rapidly to become compressive immediately outside the weld area. The hoop stresses decay more quickly with distance from the weld than do the axial stresses. The residual stress distributions obtained from the analysis are quite similar to those determined experimentally by neutron diffraction for a similar H4 weld.[1]

To better understand the mechanism of residual stress evolution in the H4 weld, the residual stress states at the end of various weld passes were determined. These stress states are shown in Fig. 7 (axial stress) and 8 (hoop stress). Eight residual stress states were plotted, corresponding to states after a layer of weld passes was deposited.

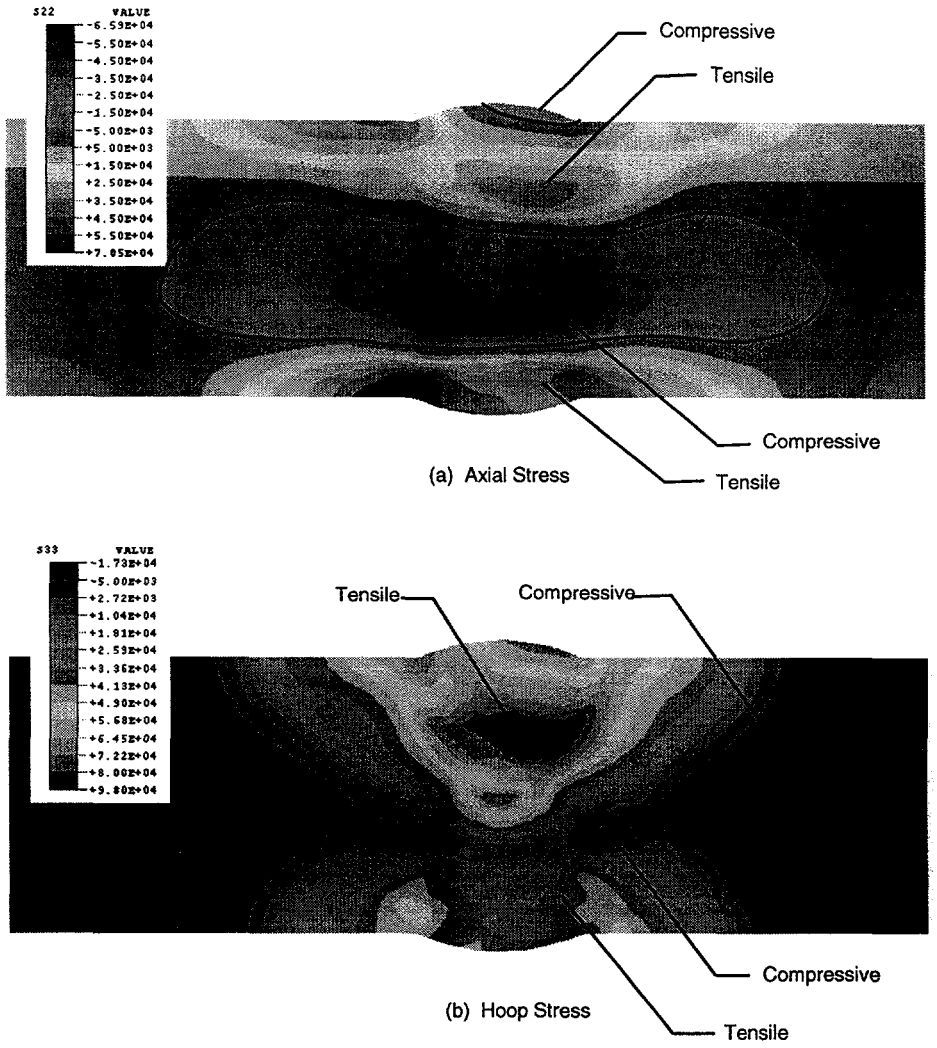

Figure 5. Contour plots of residual stress distributions in H4 weld

Both axial and hoop stresses exhibited a drastic change from Pass 9 to Pass 10. After Pass 9, the inner groove was filled, and at Pass 10 the root passes in the outer groove were started. After Pass 9, the axial stress distributions are more like a "thin-shell" type of bending distribution in which the magnitudes gradually increase from Pass 1 to Pass 9. At Pass 10, the compressive axial stress zone was pushed from the midsurface toward the inner surface, but a tensile stress zone remained at the inner surface. Thus, the characteristic, doubly curved "thick-shell" type of axial stress distribution developed. This pattern was further established at Pass 12, where the second weld layer was made in the outer groove, and maintained throughout the rest of the passes until the outer groove was filled. The same observation can also be made for the hoop stress evolution, except that tensile stresses occurred at all stages.

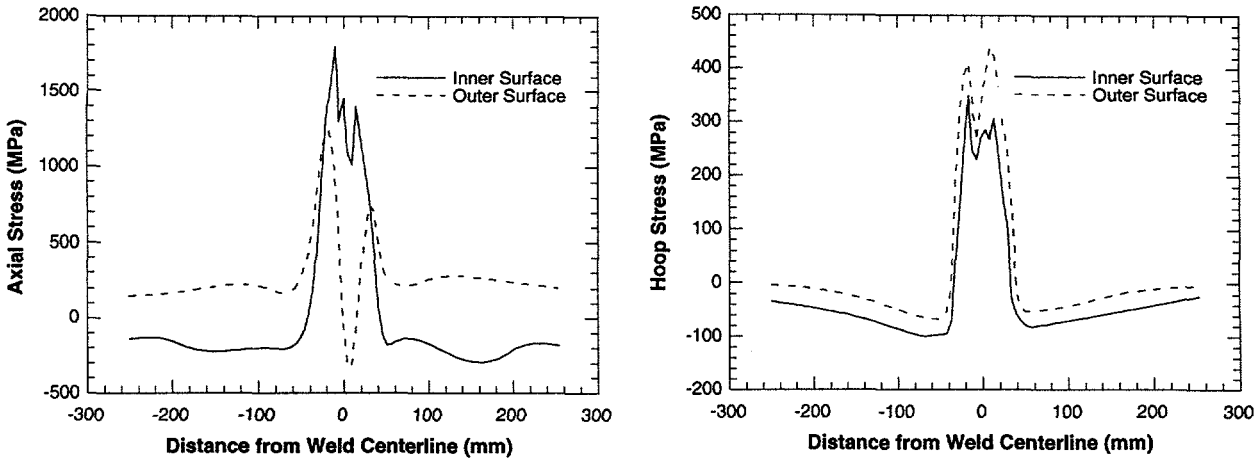

Figure 6. Residual stress distributions along inner and outer surfaces of core shroud: (a) axial stress, (b) hoop stress

Effects of Specimen Removal on Residual Stress Distributions

Residual stress measurements of core shroud welds generally require that a portion of the shroud wall which contains the weld be removed from the structure. The process of specimen removal may alter the in–situ residual stress field. The degree of relaxation depends on the size of the specimen and on the characteristics of the surrounding residual stress field. To better quantify the effects of specimen removal, the removal process was analyzed with a 3–D shell element model.

Figure 9 shows the finite–element mesh for the shell element model used in this analysis. Only one-eighth of the entire core shroud was modeled due to size limitations of the finite–element model. The finite–element mesh consists of 2001 shell elements and 2086 nodes. As in the axisymmetrical model, a refined mesh was used in and around the weld area. Eleven sectional integration points were used through the shell thickness to accurately capture throughwall stress variations. The 0.3–m x 0.4–m (12–in. x 14–in.) shroud specimen that was removed was located at the center of the shell model, as indicated in Fig. 9.

Symmetrical displacement boundary conditions were imposed in the circumferential direction at the nodes along the two edges at $\theta = 0°$ and $\theta = 45°$ As in the axisymmetrical model, all of the nodal displacements at the H3 end were fixed; those at the H5 end were left free. The shell-element analysis was also performed with ABAQUS, along with some utility programs developed at BCL. The detailed residual stress field obtained from the axisymmetrical model was mapped onto the 3–D shell element model as an initial stress field, and equilibrium iterations for the mapped residual stresses on the shell model were performed. The specimen was then removed from the model (i.e., stresses equal and opposite to those exerted on the specimen by the surrounding material were applied to obtain stress-free boundary conditions), and the resulting changes in the stress fields were computed.

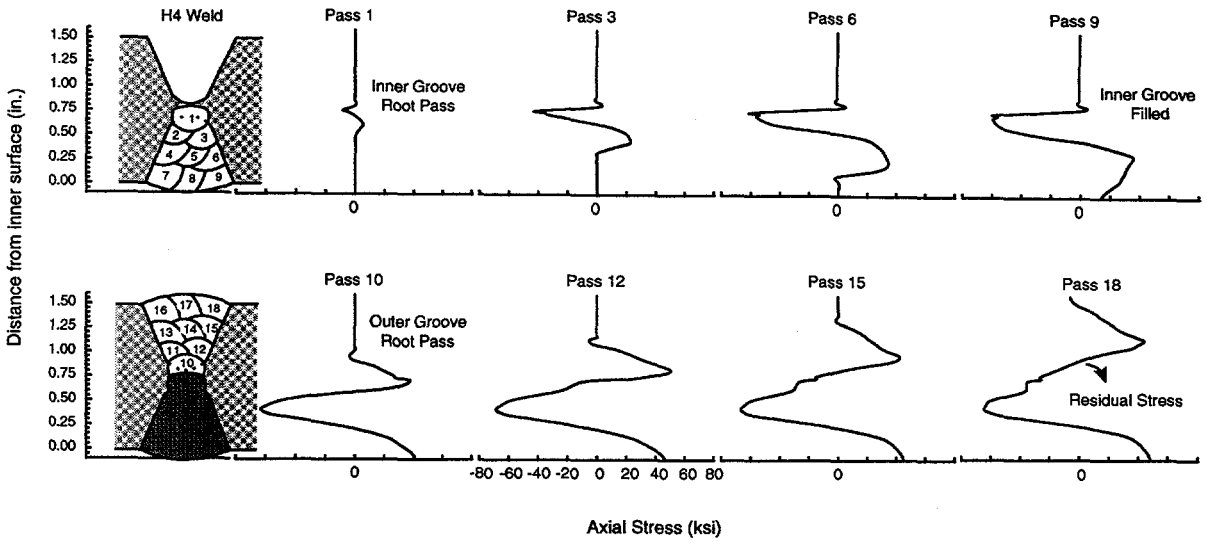

Figure 7. Evolution of axial residual stress through shroud wall at H4 weld centerline

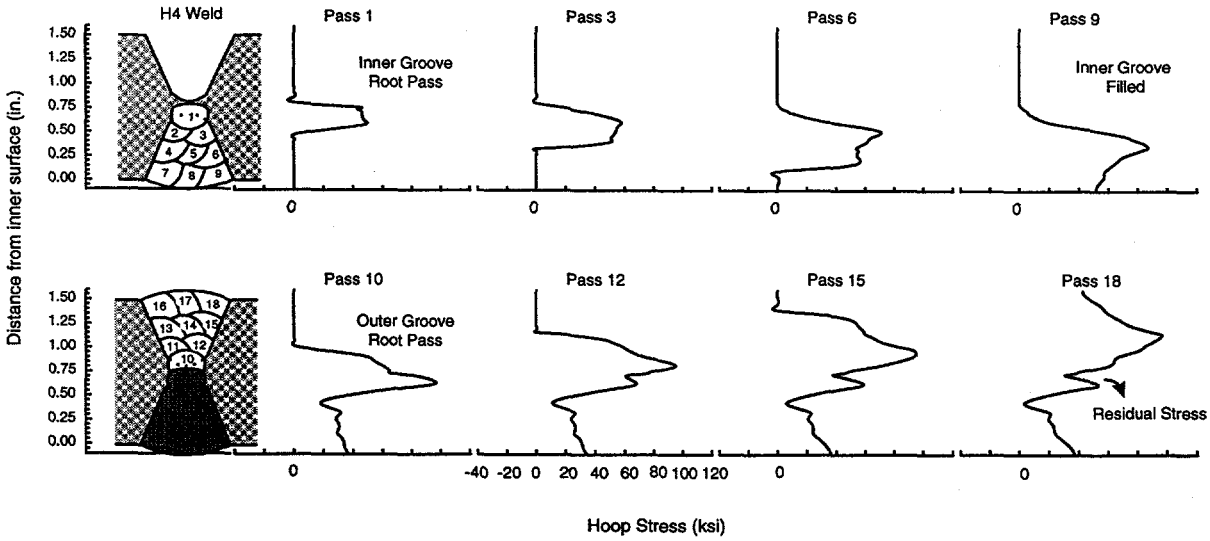

Figure 8. Evolution of hoop residual stress through shroud wall at H4 weld centerline

Figures 10a and 10b show the contour plots of axial stress distributions at the inner surface of the shroud before and after specimen removal. Note that the axial stresses are plotted with the same contour scale. After removal, the compressive axial residual stresses at the inner surface were released along two cutting edges in the hoop direction to achieve stress-free surface conditions, but the tensile axial stress at the center of specimen (in the weld) was increased (a darker color). Figures 11a and 11b show the through-thickness distributions of both axial and hoop stresses at the center of specimen before and after removal. For the axial component, both the tensile stress at the inner surface and the compressive stress at the outer surface increased. For the hoop component, however, the tensile stress at the outer surface decreased, and the tensile stress at the inner surface increased slightly. The overall changes were fairly small.

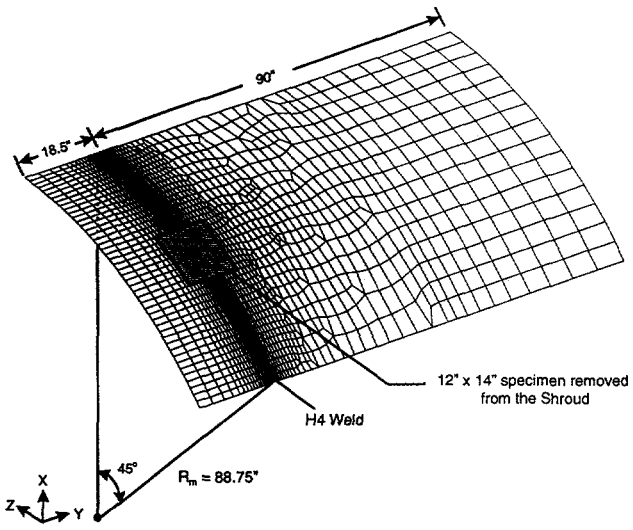

Figure 9.
3–D shell element model to evaluate effect of specimen removal on residual stress distribution in H4 weld

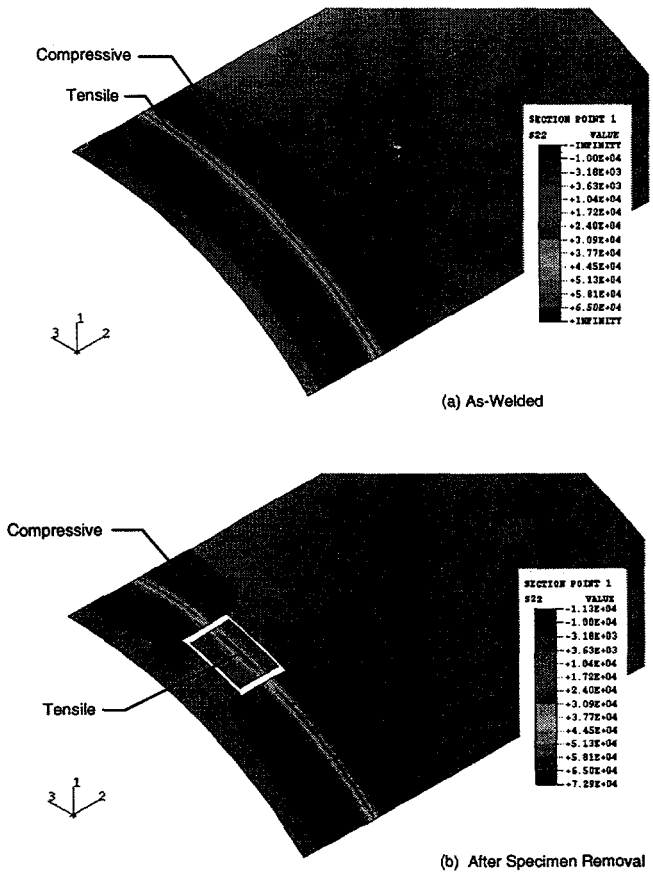

(a) As-Welded

(b) After Specimen Removal

Figure 10. Axial residual stress distribution at inner surface of core shroud

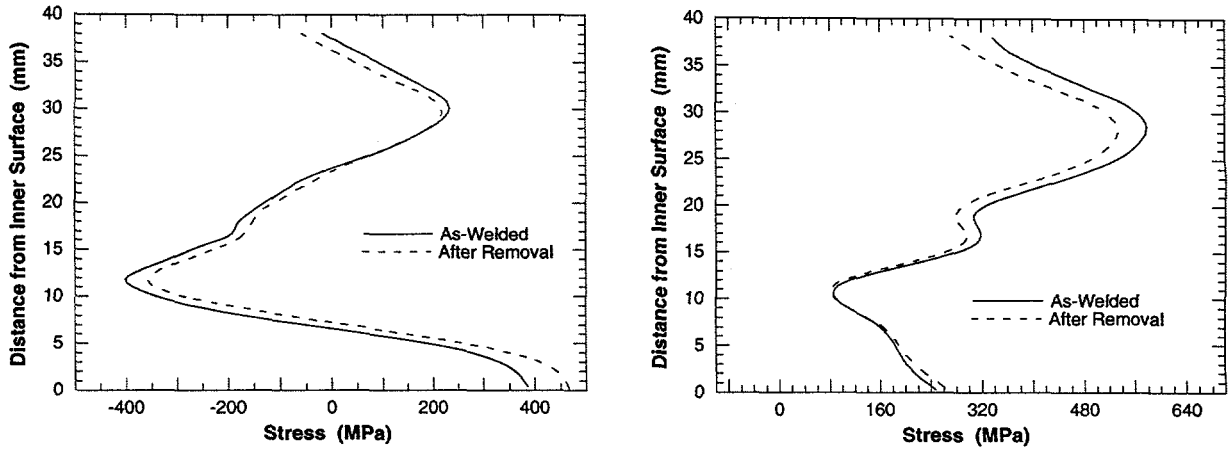

Figure 11. Throughwall residual stresses at center of a specimen removed from core shroud

The effects of specimen removal on the residual stress redistribution may be explained by the free–body diagram shown in Fig. 12. The effects of cutting along the specimen boundary can be approximately represented by equivalent sectional moments or forces obtained from the residual stress field and acting in a reversed direction. At the two circumferential cutting edges, sectional bending moments are present due to tensile axial residual stresses at the outer surface and compressive axial residual stresses at the inner surface (Fig. 6a). Along the other two edges (longitudinal cuts), sectional normal forces are present in the hoop direction and their distributions are similar to those of the hoop stresses in Fig. 6b. From the free–body diagram, it is clear that additional tensile and compressive axial stresses are introduced at the inner and outer surfaces, respectively (due to the equivalent bending moments at the circumferential cutting edges). The equivalent normal forces at the longitudinal cuts also produce a resultant bending moment at the specimen center due to the specimen curvature. This resultant bending moment causes a decrease of tensile hoop residual stress at the outer surface. Because of this relaxation, the radius of curvature of the specimen is increased after removal, as was observed experimentally for a specimen from a core shroud H4 weld.[1]

Calculation of Stress Intensity Factors for Welds with Flaws

After the residual stress distributions in the uncracked weldment were determined, the finite–element alternating method (FEAM)[2–6] was used to obtain stress intensity factors for weldments that contained flaws. FEAM methods have been verified for many different crack problems, loading conditions, etc. The major advantage of the method is that only a finite–element mesh of the uncracked geometry is needed to obtain stress intensity factors (or the J-Integral, displacements, stresses, etc.). More important, the same mesh can be used to obtain solutions for cracks of many different sizes and geometries. Because the finite–element stiffness matrix needs to be reduced only once, regardless of the crack size, crack location, crack orientation, crack number, etc., the method is extremely efficient (mixed–mode conditions can be handled as well).

The stress intensity factors due the weld residual stresses for an internal circumferential crack on the H3 side of the weld in the HAZ obtained with the FEAM are shown in Fig. 13 as a function of crack depth. The crack location (19–mm [0.75–in.] from the weld centerline on the

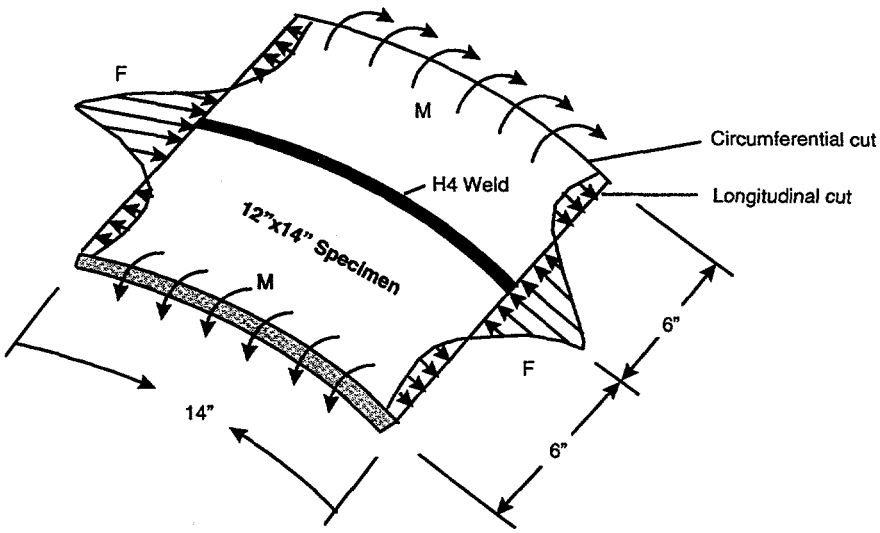

Figure 12. Equivalent boundary forces and moments on removed specimen

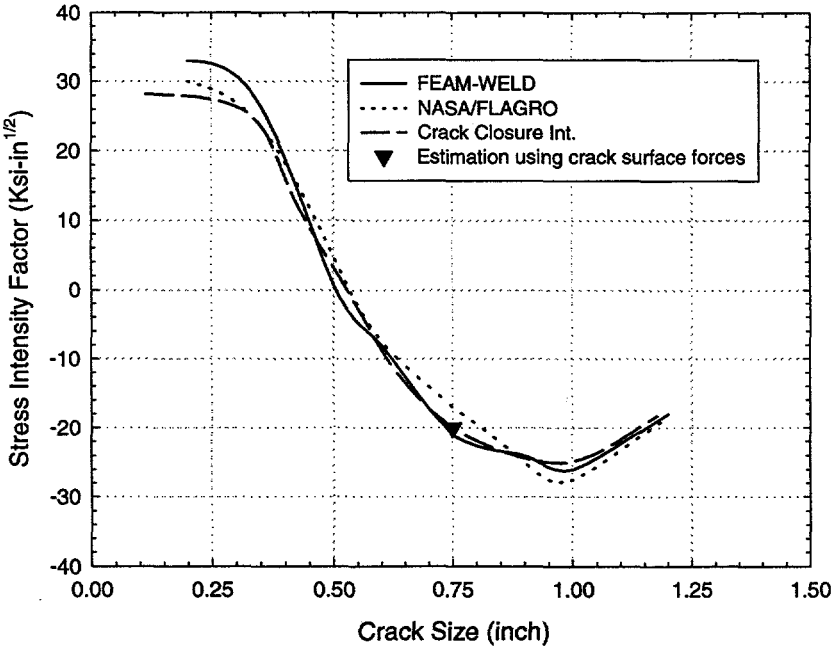

Figure 13. Stress intensity factor solutions for complete circumferential cracks in H4 weld growing from the inner surface on H3 side HAZ (19–mm [0.75–in.] from weld centerline) as function of crack depth

H3 side) is shown in Fig. 14, which also illustrates the redistribution of axial residual stresses associated with a 10.4–mm (0.41–in.) crack. The crack faces are stress–free. The stress directly ahead of the crack tip decreased to ≈138 Mpa (20 ksi). The tensile stresses at the outer surface decreased somewhat as well.

In Fig. 13, in addition to the FEAM solution, two other solutions are plotted. One solution was obtained using the NASA FLAGRO program,[7] which uses a weight function method with the crack plane residual stresses serving as the initial stress state. Another was calculated with the original crack closure integral technique.[8] The FEAM solution is probably the most accurate, although the three methods give comparable results. The stress intensity factor decreases as the crack depth increases until it reaches negative values for crack depths > ≈15–mm. This is consistent with the results shown in Fig. 14, where the stresses at the crack tip for a crack depth of 10.4–mm (0.41–in.) are decreasing and the stresses a short distance ahead of the crack tip are negative.

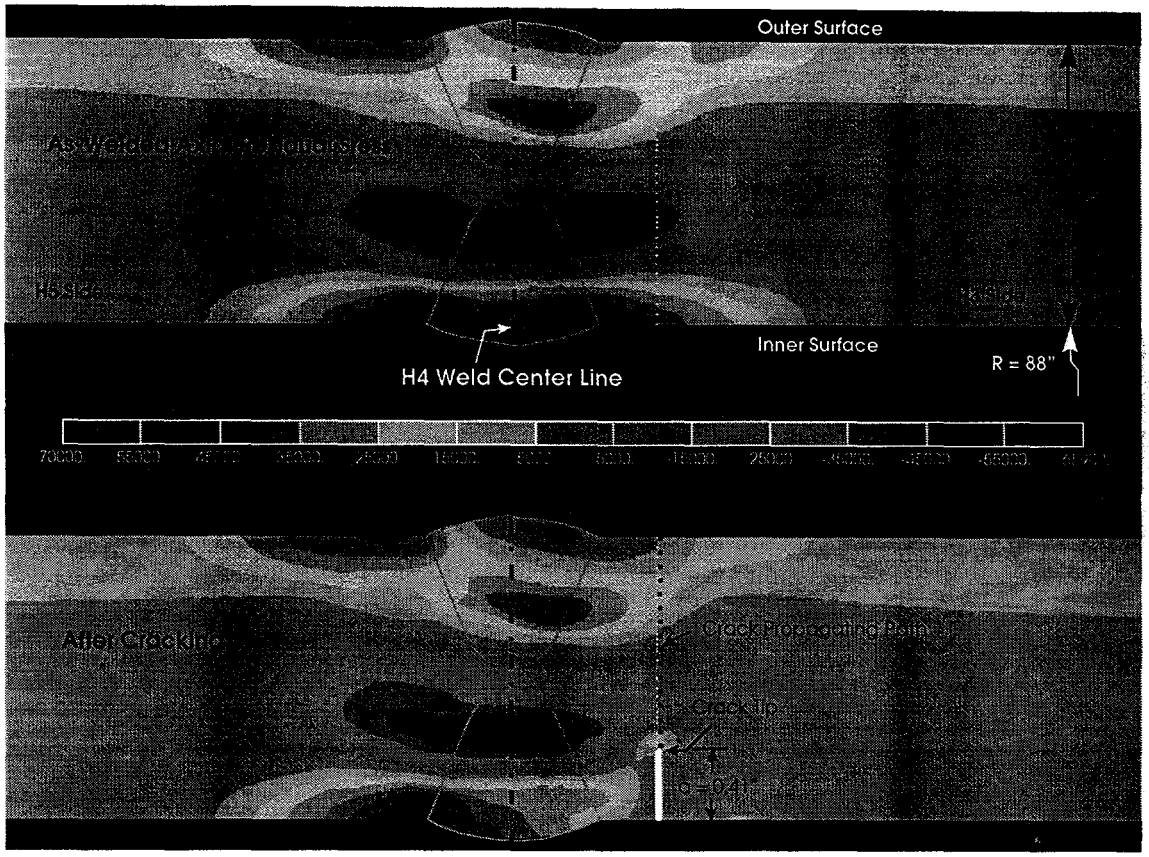

Figure 14. Redistribution of residual stress due to crack growth

The stress intensity factors for external cracks at the same axial location on the H3 side of the weld are plotted versus crack depth in Fig. 15. The variation of K with crack depth is similar to that for internal cracks both in magnitude and shape. However, the K values approach zero for a crack depth of ≈22.9–mm (0.9–in.) for the external cracks versus 15.2–mm (0.6–in.) for the internal cracks.

To analyze the case of a surface crack of length a_1, the residual stress state from the axisymmetrical case (Fig. 3) was mapped onto a 3-D model. The 3–D mesh is shown at the top of Fig. 16. For this analysis, the stresses were also assumed to be symmetrical about the weld centerline. The stresses on the H3 side of the weld were used for the symmetrical distribution. The mesh refinement in the radial and axial directions for the axisymmetrical model was greater than for the 3–D model. Hence, the mapped stresses in the 3–D model represent averages of the stresses over several elements in the axisymmetrical model, and the 3–D solution is expected to be somewhat less accurate than the solution for the axisymmetrical model. The surface crack was then introduced into the model (at the weld centerline), as illustrated in the upper portion of Fig. 16. The crack length was fixed at 88.9–mm (3.5–in.) and the crack depth, a_2 was varied. The FEAM approach was used to obtain stress intensity factors as a function of elliptic crack angle, as illustrated in the lower portion of Fig. 16. Although the stress state in the uncracked case was axisymmetrical, the stress redistribution that occurs when the surface crack is introduced is not axisymmetrical. Hence, K varies with the elliptic crack angle. An elliptic angle of 90° indicates the deepest point of the crack (at a_2) and an angle of 0° corresponds to the inner

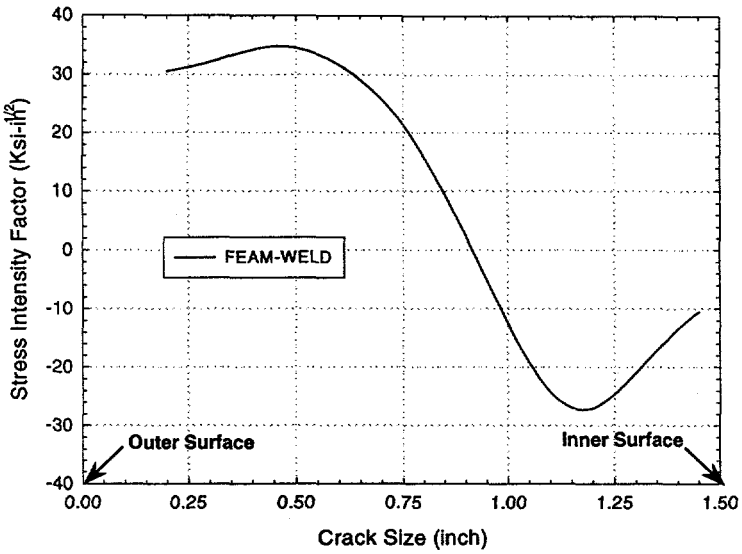

Figure 15.
Stress intensity factor solutions for complete circumferential cracks in H4 weld growing from the outer surface on the H5 side HAZ (15.5–mm (0.61–in.) from weld centerline) as function of crack depth

surface of the pipe (at location a_1). The K values at the deepest point of the crack are larger than those shown in Fig. 15 (note that a very long a_1 would represent an axisymmetrical crack). This is expected because the stresses at the weld centerline are larger than those at the H3-side HAZ crack location.

The K values at the deepest point of the crack decrease as the crack depth increases (recall that the crack length a_1 is kept constant in these calculations). However, as the crack depth increases, K increases at elliptic angles of about 40° or less. For crack depths of 10-13–mm (0.4–0.5–in.), the K at the deepest point of the crack is markedly smaller than the K near the surface of the pipe. These results suggest that cracks, if driven by corrosion mechanisms that depend on K, will tend to increase in length in the angular direction much more rapidly than they grow throughwall. Indeed, there will be a tendency for full 360° cracks to develop. For the axisymmetrical case with a complete 360° crack, the results indicate that a crack that grows from the inside to the outside of the vessel, or vice versa, would be likely to stop about midwall, because K becomes negative for deeper cracks.

References

1. E. A. Payzant, S. Spooner, X. Zhu, C. R. Hubbard, S. T. Rosinski, and J. Dowicki, *Experimental Determination of Residual Stress by Neutron Diffraction in a Boiling Water Reactor Core Shroud,* Proc. of ASME PVP Conf., Vol. 322, American Society of Mechanical Engineers, New York, pp. 55-61 (1996).

2. T. Nishioka and S. N. Atluri, *Analytical Solutions for Embedded Elliptical Cracks, and Finite-element Alternating Method for Elliptical Surface Cracks Subjected to Arbitrary Loadings,* Eng. Fracture Mechanics, **17** (3), pp. 247-268 (1983).

3. R. B. Stonesifer, F. W. Brust, and B. N. Leis, *Mixed-Mode Stress Intensity Factors for Interacting Semi-Elliptical Surface Cracks in a Plate,* Eng. Fracture Mechanics, **45** (3), pp. 357-380 (1993).

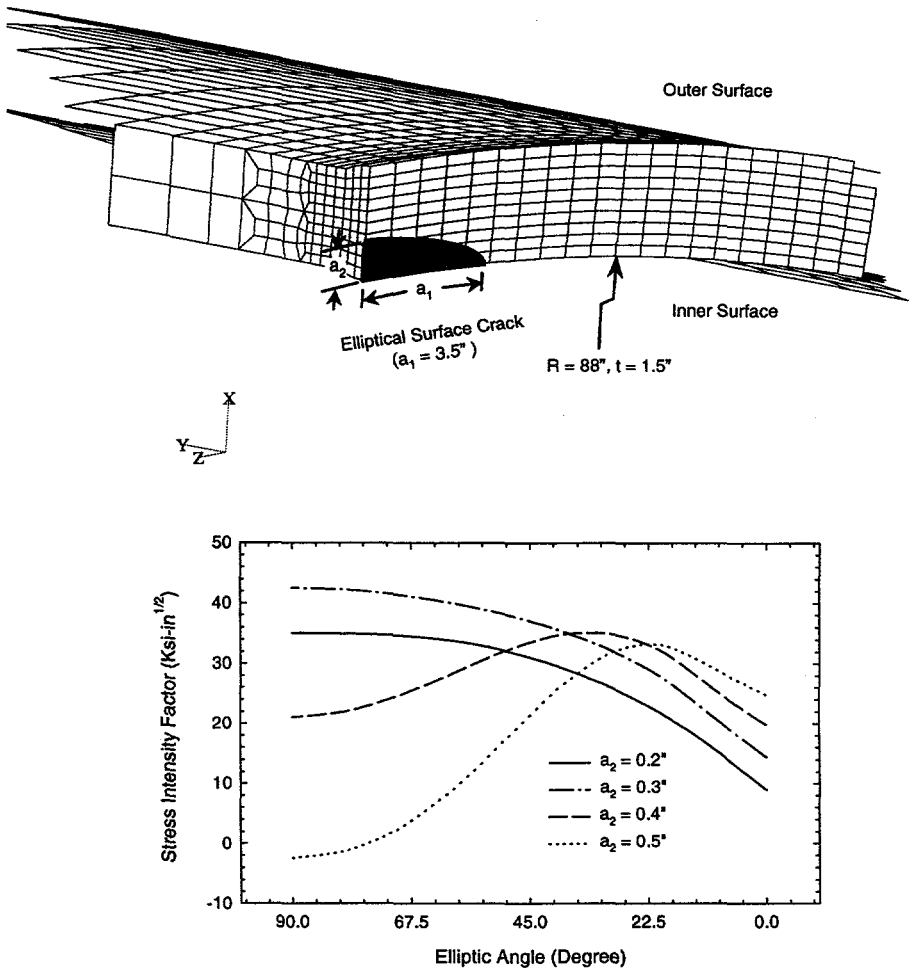

Figure 16. Stress intensity factors for surface cracks in weld centerline of H4 weld

4. R. B. Stonesifer, F. W. Brust, and B. N. Leis, *Stress Intensity Factors for Long Axial OD Surface Cracks in Large R/t Pipes*, ASTM STP 1131, American Society for Testing and Materials, Philadelphia, PA, pp. 29-45 (1992).

5. T. Nishioka and S. N. Atluri, *Analysis of Surface Flaw in Pressure Vessels by a New 3-Dimensional Alternating Method*, J. Pressure Vessel Technol., **104**, pp. 299-307 (Nov. 1992).

6. S. N. Atluri, *Energetic Approaches and Path Independent Integrals in Fracture*, in Computational Methods in Mechanics of Fracture, ed. S. N. Atluri, North-Holland (1968).

7. NASA FLAGRO Version 2.0, Developed by R. Forman, National Aeronautics and Space Administration, Dayton, OH, (1993).

8. F. G. Buchholtz, *Improved Formulae for the Finite-element Calculation of the Strain Energy Release Rate by the Modified Crack Closure Integral Method*, in Accuracy Reliability and Training in FEM Technology, J. Robinson, ed., Robinson and Associates, Dorset, England, pp. 650-659 (1984).